# TOWARDS TRAJECTORY PREDICTION AND OPTIMISATION FOR ENERGY EFFICIENCY OF AN AIRCRAFT WITH ELECTRICAL AND HYDRAULIC ACTUATION SYSTEMS

**Michael A. Cooper, Craig P. Lawson, Daniele Quaglia, David Zammit-Mangion, Roberto Sabatini**
**School of Engineering, Cranfield University, MK43 0AL, UK**
*m.a.cooper@cranfield.ac.uk*

**Keywords**: *electromechanical electro-hydrostatic servohydraulic actuator power*

## Abstract

*As part of the CleanSky programme, this paper investigates the power consumption characteristics of standard hydraulic actuation systems against the two main power by wire alternatives; electro-hydrostatic and electromechanical actuators.*

*Mathematical models are constructed for each technology which simulates the position response and power consumption of the actuators. The models are dynamic and designed with execution speed as a primary concern.*

*The difficulty with aircraft primary flight control actuator simulation is obtaining input command and load force data. One solution is to record the data from flight tests but this is costly, another solution is to use a 6 degree of freedom (6-DOF) aircraft dynamics model (ADM). This technique is much more accessible and with today's high performance computers it is easily achievable; the computing power of modern desktop PC's already accommodates the concurrent simulation of a 6-DOF aircraft with high fidelity models of subsystems.*

*The actuator models are integrated with a 6-DOF flight dynamic model of a medium range, single aisle 150 seat transport aircraft to generate control surface demands during manoeuvres. The outputs of the actuator models, in turn, generate surface responses which affect the motion of the aircraft.*

*The aerodynamic force is estimated using textbook methods for two dimensional aerofoils, programmed into a series of lookup tables that run continuously with the 6-DOF and actuator models. The aero load estimator generates hinge moments as a function of aircraft speed, angle of attack, altitude and surface deflection as well as static wing geometry data.*

*This allows the aircraft to fly a pre-determined route using an autopilot and facilitates the analysis of the power consumed by the actuation systems during that route. By tuning the manoeuvre parameters such as bank angle and rate, it is hypothesized that a reduction in energy consumption can be achieved by executing manoeuvres in such a way that the actuators operate in their most efficient states more regularly. Whilst the magnitude of the savings may not be large, it will be simple to implement and of some value.*

## 1 Background

The quest for the all electric aircraft is currently a strong area of research in the field of aerospace engineering. The concept of replacing the hydraulic actuation system, bleed air ice protection system (IPS) and environmental control system (ECS) with electrically powered alternatives has the capability to conserve energy and reduce the maintenance costs on aircraft operators [1]. Energy reductions are generally achieved by the greater controllability of fully electric systems; heat can be applied precisely where needed in the case of de-icing and electric actuation systems avoid having to maintain a continuously pressurised circuit.

There is also a benefit to the propulsive efficiency of the turbine engines; by replacing the pneumatic power off-take from the engines with a single (albeit larger) mechanical off-take, the engines operate more efficiently.

These systems also deliver significant maintenance advantages to aircraft operators since electrical systems do not suffer from the reliability issues inherent with containing pressurised fluids. Electrically powered actuators have been shown [2] to have the benefit of directly replaceable parts which can be swapped without having to drain and flush the hydraulic supply lines. Van den Bossche implemented a modular system where the less reliable power electronics of an electro-hydrostatic actuator can be replaced separately to the more reliable hydraulic cylinder; this lowers maintenance costs by avoiding replacement of serviceable subcomponents.

This work is similar to previous work by Di Rito et al. [3], where the three actuation systems are modelled and analysed using fixed time series input data, but differs by constructing the models using fundamental equations since it allows greater flexibility to tune simulation fidelity and execution speed. This paper extends the prior work by combining the actuation systems with a 6-DOF model to remove the dependency on having externally generated command signals.

The complete model is designed to be used in the context of a trajectory optimisation tool which calculates optimal (in terms of noise, fuel, range etc.) flight paths between city pairs. The complete tool models an aircraft and its propulsion system (including emissions), IPS, ECS, electrical power consumers and can plot trajectories which obey air traffic management constraints such as those set out under the SESAR programme.

## 2 Actuator Models

The first step in creating the power estimation tool is modelling the actuators; for this study the two most prominent electrically powered actuator technologies (electromechanical and electro-hydrostatic) are compared against the classic electro-servohydraulic actuators.

The incentive is to obtain models which represent the dominant dynamics of the actuators, but reducing complexity where appropriate to trade detailed fidelity for execution speed. As a general guide, the models are considered acceptable if they achieve a speed at least 10 times faster than real time on a single threaded 3.4 GHz Intel desktop processor.

The power consumed by the actuators above the output piston power is caused by the inefficiencies in the system. In a physical system this is typically caused by the friction between moving parts, but it also includes fluidic losses in hydraulic systems and magnetic losses in motors. Since the focus of this work is on the power consumption, the modelling of the losses becomes key. Friction models can take many forms from straightforward viscous friction to full nonlinear breakaway, Stribeck, Coulomb and viscous models. The accuracy achieved by the latter example is beneficial in actuator modelling since the system regularly changes direction, but the discontinuity added at the crossover point slows down the simulation significantly. For this reason the mechanical components' friction is modelled by a continuous $\tanh(x)$ approximation of Coulomb friction with viscous friction to ensure fast crossover solutions during simulation.

Each model is designed to accept vector inputs to represent the aileron, elevator and rudder actuators in parallel for computational efficiency. Since the intended focus of the trajectory optimisation is on typical use, possible failure modes are ignored and thus power losses in backup actuators in damping mode and redundant power supply circuits are not considered.

### 2.1 Electro-servohydraulic Actuator

The electro-servohydraulic (ESH) actuator consists of a symmetrical hydraulic cylinder connected to a 3000 psi hydraulic power supply through an electrically signalled servo valve. The operation is simple: the servo valve controls the flow to the cylinder chambers allowing speed and direction control. This type of actuator has seen widespread use in the

commercial aviation industry since the inception of fly-by-wire technology, but there is significant complexity in the design, installation and maintenance of a triplex hydraulic system.

However, there is also a cost in efficiency associated with the continuously pressurised system, since the servo valves are always exposed to the supply pressure a continuous leakage flow is induced.

The valve, cylinder and power supply are modelled separately, but the valve and cylinder used as a pair make a complete actuator. A single power supply model for the whole system is used which represents the combined capacity of both engine driven pumps.

## Cylinder

The conventions used for the hydraulic cylinder are shown in Fig. 1.

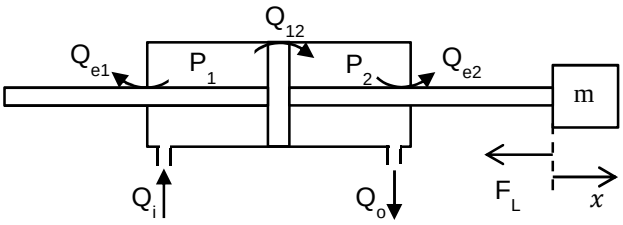


**Fig. 1. Modelling diagram of a symmetrical hydraulic cylinder.**

The cylinder is modelled using the continuity equation for compressible flows to represent the cylinder chambers:

$$\sum Q_{in} - \sum Q_{out} = \frac{dV_0}{dt} + \frac{V_0}{\beta_e}\frac{dP}{dt} \qquad (1)$$

Where $Q$ is the flow rate, $V$ is the chamber volume (at zero pressure) and $\beta_e$ is the bulk modulus of the fluid. With reference to the work published by Dinca et al. [4] the cylinder is first represented by two chambers, each described by equation 1:

$$\frac{dP_1}{dt} = [Q_i - Q_{12} - Q_{e1} - \dot{x}A_c]\frac{\beta_e}{V_1} \qquad (2)$$

$$\frac{dP_2}{dt} = [-Q_o + Q_{12} - Q_{e2} + \dot{x}A_c]\frac{\beta_e}{V_2} \qquad (3)$$

where $A_c$ is the piston area.

Equations 2 and 3 can be implemented in this form for the most realistic simulation, but practise shows the equations cause pressure oscillations between each other and require small simulation steps to capture the motion. For this reason, equations 2 and 3 are combined to form an expression for the pressure difference across the piston in equation 4, where the leakage flow $Q_{12}$ has been replaced by a linear approximation for laminar flow conditions with leakage coefficient $C_{12}$. Equation 4 lends itself to faster execution of the cylinder model since the high frequency interaction between the two chambers is avoided.

$$\frac{d(P_1 - P_2)}{dt} = [2Q_i - 2C_{12}(P_1 - P_2) - 2\dot{x}A_c]\frac{\beta_e}{V} \qquad (4)$$

There are limitations in representing the circuit in this way: an accumulator or charge pump is usually connected to the circuit using check valves which ensure each side of the circuit is kept above a minimum pressure. Equation 4 does not facilitate unsymmetrical pressure behaviour across the cylinder and so precludes the use of an accumulator. Equation 4, however, does allow the pressure integrator to have a saturation limit applied to simulate pressure release valves opening in an overpressure condition (typically by applying too much load force).

The pressure across the cylinder is applied to the mechanical model of the piston given in equation 5, which models the motion of the piston mass.

$$A_c(P_1 - P_2) = m\ddot{x} + B_v\dot{x} + F_L \qquad (5)$$

where $m$ is the piston mass, $B_v$ is the piston damping and $F_L$ is the load force.

## Hydraulic Power Supply

The hydraulic power supply is also modelled using equation 1 [5], applying it to the volume of fluid in the pipes between the engine driven pumps and servo valves $V_t$:

$$\frac{dP_s}{dt} = [Q_P - Q_L]\frac{\beta_e}{V_t} \qquad (6)$$

The flow rate capacity of the pump is defined using $Q_p$ and the total load flow rate supplied to the whole system is $Q_L$. The pressure integrator is limited to the system design pressure (often 3000 psi), so the model will maintain the optimum pressure until more flow is drawn than the pump is capable of supplying. At this point the pressure will decrease until the load flow falls to within the pump capacity.

**Servo Valve**

The final significant component is the servo valve, which controls the flow to the cylinder. The type chosen is the two stage nozzle-flapper spool valve shown in Fig. 2. This was chosen on the basis of its frequent use in aerospace designs. A torque motor is used to control a hydraulic amplifier, which in turn moves the spool. The position of the spool controls which output port is connected to the supply pressure, which is connected to tank as well as the flow rate through the valve. The torque motor is modelled as a series LR circuit with inductance $L_t$ and resistance $R_t$:

$$\frac{I(s)}{V(s)} = \frac{1}{sL_t + R_t} \tag{7}$$

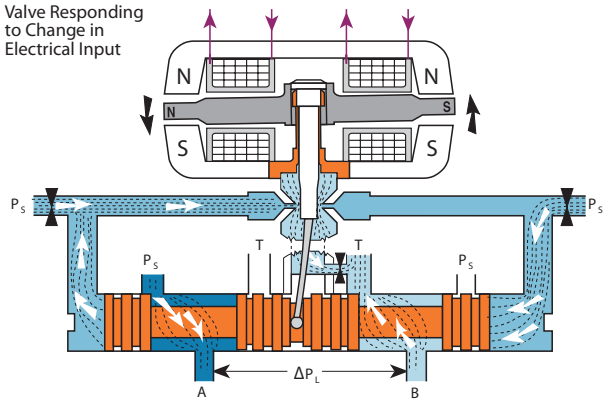


**Fig. 2. Diagram of torque motor and spool when responding to a change in electrical input [5].**

The servo valve spool dynamics are modelled using a standard second order transfer function as recommended by Moog [6]:

$$\frac{Q(s)}{I(s)} = \frac{\omega_n^2}{s^2 + 2\zeta\omega_n s + \omega_n^2} \tag{8}$$

Equation 8 gives the flow rate at the rated pressure drop (cylinder pressure of 2/3 the supply pressure), which needs to be regulated based on the actual pressure drop. This adjustment is carried out using the orifice flow equation in (9).

$$Q_L = Q_R I_V^* \sqrt{\frac{\Delta P_V}{\Delta P_R}} \tag{9}$$

This equation relates load flow $Q_L$ to rated flow $Q_R$ using the square root of the pressure dropped across the valve $\Delta P_V$ (normalised to the rated pressure $\Delta P_R$) and $I_V^*$, the current flow to the torque motor normalised to the saturation current.

The final task is to calculate the powers at various locations in the system, from the mechanical power delivered by the piston to the mechanical shaft power required from the engine power off-take shaft to drive the hydraulic supply. The equations to calculate these powers are given in Tab. 1.

| | |
|---|---|
| $P_{engine}$ | $P_{fluid(total,all)}/\eta_{vdp}$ |
| $P_{fluid(total)}$ | $P_S Q_L$ |
| $P_{fluid(valve)}$ | $(P_s - \Delta P)Q_L$ |
| $P_{fluid(cylinder)}$ | $\Delta P Q_L$ |
| $P_{piston}$ | $F_L v$ |

**Tab. 1: Formulae used to calculate power at various locations in the ESH system.**

Where: $P_S$ is the supply pressure, $\Delta P$ is the pressure across the cylinder, $F_L$ is the force applied to the load, $v$ is the velocity which the load is moved at and $\eta_{vdp}$ is the efficiency of the engine shaft to hydraulic power conversion.

## 2.2 Electromechanical Actuator

Electromechanical (EM) actuators have been used in industry for many years in low power capacities providing general work such as door opening and process control. The basic design is a DC motor providing torque to a ball screw through a gearbox, which converts rotatory motion to linear motion.

Electromechanical actuators are potentially the most efficient of the two electrical technologies available for aerospace use with highly efficient motors and ball screws composing the key parts. The benefits are not

without their costs however. The tight tolerances required to manufacture such an efficient ball screw naturally mean the drive is very susceptible to dirt and ice ingress. Small amounts of contamination can lead to severe malfunctions that are difficult and costly (both in weight and financial terms) to provide true redundancy for. Challenges aside, progress has been made in the community on providing suitable jam prevention mechanisms and as such it is considered beneficial to include EM technologies in the comparison.

The generalised diagram representing the EM actuator is shown in Fig. 3.

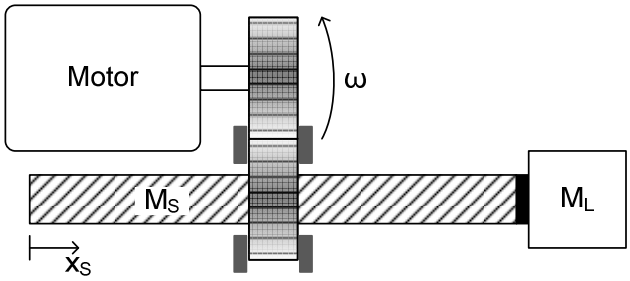


**Fig. 3. Diagram of motor, ball screw and load mass configuration.**

The motor chosen is a brushless DC motor as it exhibits good control characteristics and high efficiency. The electrical circuit is represented using equation 10 and the mechanical components with equation 11.

$$\frac{di}{dt} = \frac{1}{L}(V - iR - K_v\omega) \tag{10}$$

$$\frac{d\omega}{dt} = \frac{1}{J}(K_t i - B\omega - T_L) \tag{11}$$

Where $V$ is the applied voltage, $L$ is the coil inductance, $i$ is the coil current, $R$ is the coil resistance, $K_v$ is the velocity constant, $\omega$ is the angular velocity, $J$ is the rotor inertia, $K_t$ is the torque constant, $B$ is the viscous damping and $T_L$ is the load torque. The motor connects to a ball screw through a gearbox which reduces the angular velocity before converting it to linear motion. The gearbox is considered to be of high quality with no significant backlash, simplifying the equations for fast execution. The mechanical ball screw and load are considered as a 2-DOF system based on a modified version of the model created by Du et al. [7] as shown in Fig. 4.

The dynamics of the masses are described by equations 12 and 13 and the load torque on the motor is given by equation 14.

The final part of the electro-mechanical actuator model is the equations which calculate the power consumption at each stage, given in Tab. 2.

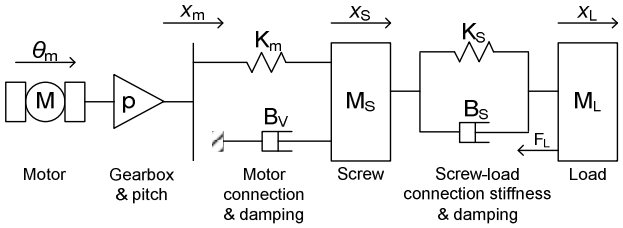


**Fig. 4. Equivalent schematic diagram of EM actuator.**

$$\ddot{x}_S = \frac{1}{M_S}\big(-B_V\dot{x}_S - B_S(\dot{x}_S - \dot{x}_L) + K_m(p\theta_m - x_S) - K_S(x_S - x_L)\big) \tag{12}$$

$$\ddot{x}_L = \frac{1}{M_L}(+B_S(\dot{x}_S - \dot{x}_L) + K_S(x_S - x_L) - F_L) \tag{13}$$

$$T_L = pK_m(p\theta - x_s) \tag{14}$$

| | |
|---|---|
| $P_{electrical}$ | $VI$ |
| $P_{motor}$ | $T\omega$ |
| $P_{piston}$ | $F_L v$ |

**Tab. 2: Formulae used to calculate power through the EM model.**

## 2.3 Electro-hydrostatic Actuator

The electro-hydrostatic actuator consists of, in its most basic form, a variable speed servo motor, a fixed displacement pump and a symmetrical cylinder. The motor and pump provide flow directly to the cylinder and the linear velocity is proportional to the motor speed. With the direct coupling between the motor and cylinder, position control becomes an extended motor control problem.

The electro-hydrostatic actuator is the most straightforward actuator to retrofit onto current aircraft since the cylinders attached to the control surfaces are very similar to (or the same as) their ESH counterparts. This allows straightforward jam prevention by opening a bypass valve to enable damping mode.

The EH actuator uses the same DC motor model that is used for the EM actuator in equations 10 and 11. The flow rate output of the fixed displacement pump is modelled using equation 15.

$$Q_p = D\omega \tag{15}$$

Where $D$ is the pump displacement and $\omega$ is the motor angular velocity. Using the notation in Fig. 1, the leakage flow past the piston $Q_{12}$ (due to pressure difference across the piston head) is assumed to be laminar and expressed as a linear function of the leakage coefficient $C_{12}$:

$$Q_{12} = C_{12}(P_1 - P_2) \tag{16}$$

The cylinder model used for the EH actuator is similar to that used for the ESH actuator in equation 4, but with the supply replaced by equation 15. Hence,

$$\frac{d(P_1 - P_2)}{dt} = [2D\omega - 2C_{12}(P_1 - P_2) - 2\dot{x}A]\frac{\beta}{V} \tag{17}$$

The piston dynamics are represented with equation 5 in the EH model since it is identical the to the ESH piston. The load torque on the motor is then calculated using a linear approximation for pump efficiency $\eta_p$:

$$T_L = \frac{D}{\eta_p}(P_1 - P_2) \tag{18}$$

Finally, the power consumptions are calculated using Tab. 3.

| | |
|---|---|
| $P_{electrical}$ | $VI$ |
| $P_{motor}$ | $T\omega$ |
| $P_{fluid}$ | $\Delta P Q_L$ |
| $P_{piston}$ | $F_L v$ |

**Tab. 3: Formulae used to calculate the powers through the EH actuator.**

## 2.4 Control Surface Model

To covert the motion of the linear actuators to control surface deflections, the geometric parameters need to be derived into an equation which relates the actuator displacement $x$ to the control surface deflection $\delta$. The surface model is not required to transmit force/torque, since the aerodynamic loads are generated separately and are applied as linear forces to the actuator models directly. The mechanical installation schematic shown in Fig. 5 gives the notation used for the equations which relate the output to the input. Note that a subscript 0 denotes a position or angle at neutral (central) deflection.

The length $b$ changes with actuator extension and is calculated using:

$$b = x + b_0 \tag{19}$$

Lengths $a$ and $c$ are fixed so the cosine rule can be used to calculate $\beta$:

$$\beta = \cos^{-1}\left(\frac{b^2 - c^2 - a^2}{-2ac}\right) \tag{20}$$

Finally, the surface deflection is calculated using the neutral position $\beta$ angle:

$$\delta = \beta - \beta_0 \tag{21}$$

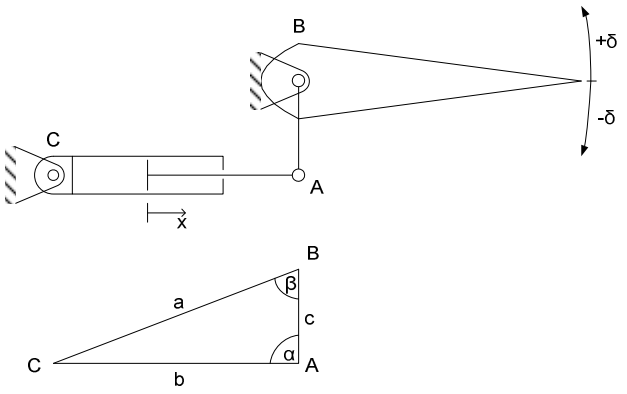


**Fig. 5. Diagram showing the notation used for the actuator-control surface installation.**

## 3 6-DOF Model

The aircraft model is implemented using 6-DOF equations of motion with the input forces and moments equated using dimensionalised aerodynamic coefficients. The model coefficients are derived from DATCOM, providing reasonable data throughout the

subsonic speed regime but becoming less accurate towards the cruising speed of the case study aircraft of Mach 0.78. Although undesirable, this cannot be avoided since supplemental wind tunnel data is not available and detailed computational fluid dynamic (CFD) studies are beyond the scope of this work.

An aircraft can be modelled as a variable mass rigid body which is subject to propulsive, aerodynamic and gravitational forces. The motion of the aircraft is then defined by the position and velocity of its centre of gravity, orientation angles and angular rates of the body reference frame with regard to an inertial frame. The equations describing the motion of the aircraft are derived from Newton's second law:

$$\begin{aligned}\sum Forces &= \left.\frac{d(m*V^b)}{dt}\right|_i = m\left.\frac{dV^b}{dt}\right|_i + V^b\frac{dm}{dt}\\ &= m\left(\left.\frac{dV^b}{dt}\right|_b + \omega\wedge V^b\right) + V^b\\ \sum Moments &= \left.\frac{d(m*H)}{dt}\right|_i = m\left.\frac{dH}{dt}\right|_i + H\frac{dm}{dt}\\ &= m\left(\left.\frac{dH}{dt}\right|_b + \omega\wedge H\right)\end{aligned} \quad (22)$$

where:

H = Kinematic moment of the aircraft in the body frame.

$V^b = [u \quad v \quad w]^T$, velocity with regards to the inertial frame, expressed in the body frame.

$\omega = [p \quad q \quad r]^T$, body axis angular rates.

m = Aircraft mass.

The assumptions made in constructing the 6-DOF model are the following:

- The earth model chosen is the WGS-84 model, which approximates the earth as an ellipsoid.
- The atmospheric model is the International Standard Atmosphere, considered at rest relative to the Earth. Temperature, pressure and density are considered to be a function of altitude.
- The aircraft is considered as rigid and with a right-left plane of symmetry.
- Forces acting on the center of gravity of the aeroplane are the thrust, aerodynamic forces and the weight.

A simple autopilot is installed, which controls the altitude, heading, airspeed and yaw damping. The flight controller is designed to adhere to typical manoeuvre conventions, such as limiting the change of heading to a maximum rate of 3°/s and limiting the maximum climb and descent rates for passenger comfort. The most important feature of the autopilot is the ability to explicitly state the desired bank angle achieved during a banked turn. It is through this that the manoeuvre rates will be varied and optimised, with lower bank angles expected to require lower forces from the actuators and vice versa.

Low bank angle turns have the obvious effect of increasing the radius of the turn and the time the aircraft spends at a wings banked attitude. In this state the aircraft needs to pitch up slightly and also increase thrust to remain in a level coordinated turn at constant speed.

To quantify the effect the actuator-optimal manoeuvres have on the energy consumption of the entire aircraft, a simple engine model is constructed using a first order lag. This uses a lookup table to estimate thrust at a range of altitudes and airspeeds, and then uses data from the BADA database [8] to estimate fuel burn for the high bypass ratio turbofan engines during cruise. It should be noted that the fuel burn estimates are solely based on the fuel burnt due to the thrust generated; it does not include a means of relating aircraft secondary power off-takes to fuel burn. Due to this limitation the fuel burn values are only useful to represent the change in fuel penalty with reference to some baseline manoeuvre and not a direct measure of how much fuel is saved with electric actuators.

## 4 Aero Load Estimator

Aerodynamic load estimation is a complex task which becomes highly nonlinear towards the

$$c_{h_\alpha} = \left\{ \frac{{c_{h_\alpha}}'}{\left(c_{h_\alpha}\right)_{theory}} \cdot \left(c_{h_\alpha}\right)_{theory} + 2\left(c_{l_\alpha}\right)_{theory} \cdot \left[1 - \frac{c_{l_\alpha}}{\left(c_{l_\alpha}\right)_{theory}}\right] \cdot \left[tan\frac{\Phi''}{2} - \frac{t}{\bar{c}}\right] \right\} \cdot \frac{\left(c_{h_\alpha}\right)_{bal}}{{c_{h_\alpha}}''} \cdot \frac{1}{\sqrt{1-M^2}} \quad (23)$$

$$c_{h_\delta} = \left\{ \frac{{c_{h_\delta}}'}{\left(c_{h_\delta}\right)_{theory}} \cdot \left(c_{h_\delta}\right)_{theory} + 2\left(c_{l_\delta}\right)_{theory} \cdot \left[1 - \frac{c_{l_\delta}}{\left(c_{l_\delta}\right)_{theory}}\right] \cdot \left[tan\frac{\Phi''}{2} - \frac{t}{\bar{c}}\right] \right\} \cdot \frac{\left(c_{h_\delta}\right)_{bal}}{{c_{h_\delta}}''} \cdot \frac{1}{\sqrt{1-M^2}} \quad (24)$$

full extent of travel. A complete estimator which includes these regions would be a challenging task, requiring flight or wind tunnel testing or CFD analysis. These are either slow, expensive or both and do not provide justifiably useful data when considering an aircraft working in normal operating conditions which is the scope of this work. Generally speaking, the flight control system is designed to keep the surfaces working in the linear region to ensure both a predictable response and to minimise stresses on the airframe.

The chosen method to estimate aero loads is by programming a software version of the hinge moment estimation equations published by Roskam [9] and utilised by Scholz for the preliminary sizing of actuators [10]. This involves digitising the lookup tables used and applying curve approximation to fit a polynomial function to each data set. Multidimensional lookup tables are avoided to provide flexibility in mapping of the source data. Indeed, the data in Roskam is not completely consistent; not every figure provides data across the same ranges of angle of attack and Mach as every other figure. Programming the polynomials individually allows the most control and has lower code overheads by avoiding Simulink's lookup table blocks. Interpolation is provided between the data plots, ie: figures that have trend lines for Mach 0.6 and 0.8 can estimate values anywhere between this range. Some data requires logarithmic interpolation and this is provided too.

The estimation is based on wing and control surface geometry, altitude, airspeed and deflection angles. The user is required to provide basic information on the aerofoils such as thickness ratio, chord and surface area.

The tool is designed to model the linear range of aero load only, around ±20° so the power estimations produced when the surfaces travel beyond this limit become unreliable.

The 2D control surface hinge moment derivative due to angle of attack is given by equation 23.

The 2D control surface hinge moment derivative due to control surface deflection is given by equation 24.

All coefficients used in equations 23 and 24 are retrieved from Roskam [9] (Vol. VI section 10.4.) Only four of the ten coefficients vary with flight condition, the remaining six are based solely on the aircraft geometry.

For efficiency, the aero load estimator is implemented as a two part module, firstly requiring a script to be executed before running the model to compute the static parameters. Secondly, the parameters which vary during a flight are implemented in custom made lookup tables in Simulink.

The two derivatives are used to calculate the hinge moment coefficient $c_h$ using equation 25 with the angle of attack $\alpha$ and surface deflection $\delta$,

$$c_h = c_{h_\alpha}\alpha + c_{h_\delta}\delta \quad (25)$$

before being dimensionalised to obtain a hinge moment (torque) in equation 26. This load torque is converted to a linear force on the actuators using the length $c$ from the control surface model. $q$ is the dynamic pressure, $A_w$ is

the top down profile area of the control surface and $\bar{c}$ is the mean chord of the control surface.

$$HM = c_h \cdot q \cdot A_w \cdot \bar{c} \qquad (26)$$

## 5 Integrating and Controlling the Aircraft and Systems Models

The actuators, aero load estimator and 6-DOF are connected in such a way that generally, the change in force and moment applied to the 6-DOF can be described by:

$$\delta F, \delta M = f(\delta, HM)$$

where $\delta$ is the control surface' deflections and $HM$ are the hinge moments applied by the airflow.

Actuator control is of primary importance when integrating the actuator models with the 6-DOF model. After many trials with different control strategies, the experience gained is that the controller behaviour has a significant effect on the simulation speed of the integrated model.

This can be attributed to several factors, the most dominant being that the actuators operate best with a stiff solver such as Simulink's *ode23tb* and the 6-DOF aircraft model executes most efficiently with a regular variable step solver such as Simulink's *ode45*. The combination requires a lot of testing of the solvers and solver options to get the best combination of speed and accuracy.

The second issue is that aerodynamic load estimates are generated using the control surface angle output from the *previous* timestep. This induces a delay between the position of the surface and the load force applied to it. With suboptimal control algorithms such as PID, which rely on an error signal, the oscillations evident in the response cause a significant slow-down in execution speed. This issue is exacerbated by the cascaded control loops with the actuator control inner loops and aircraft autopilot outer loops.

The problems induced by the load estimation lag are worsened by implementing a simple PI control structure to the actuators. This technique is acceptable with constant load force, but once the gains have been tuned at a certain load the response varies widely at different loads. Depending on how high the gains are set, the response can even become oscillatory. Generally speaking, high gains in the controller may allow tighter control of the actuator positions, but the high frequency oscillations induced cause a severe decrease in simulation speed. This is due to the smaller time steps required by the variable step solver. The authors have found the best trade-off to be setting the gains as low as possible while still achieving acceptable performance.

Reliable simulation (meaning stable and predictable simulation times irrespective of flight condition or manoeuvres undertaken) has been achieved by using the servo control advice from Parker Hannifin [11], using load force feedforward with a proportional-integral-velocity (PIV) control structure. The feedforward allows the actuator controller (either motor or servo valve) to respond to the load force without an error signal being present. This alone brings a significant improvement to the stability of the controller across the range of load forces. The PIV control structure is used because it allows greater flexibility in tuning the response; with PID the rise time and overshoot are directly linked to the proportional gain so it is not possible to achieve fast response and minimum overshoot. The PIV technique reduces the coupling between rise time and overshoot, allowing the controllers to be tuned to give a small tracking delay error, good step response performance with zero overshoot.

Having zero overshoot improved overall simulation efficiency markedly. The execution speed of the model is shown in Tab. 4 using the *ode23tb* solver for the test case described in section 6. Times are measured as the average of five 500 second runs executed serially (not using Matlab's multithreaded *parfor* loop).

## 6 Demonstration Test Case

In order to demonstrate the functionality of the complete model, an academic test case is created which consists of a series of random turns and a descent of 1000m from a cruise condition of Mach 0.78 at 10000m altitude. For investigative purposes, the descent is flown at

constant true air speed to accentuate the moving trim position required of the elevator as it descends; this increases the steady state hinge moment on the surface and the power demanded of the actuators connected to it.

The aircraft trajectory, Euler angles, actuator deflections and powers are shown in Figs. 6-9. Figs. 8 and 9 are of particular interest; they show the power consumption estimates for the actuators as the aircraft executes the manoeuvres. The plots in Fig. 8 have been scaled on the y-axis to focus on the continuous power draw while holding a load at zero velocity. In most situations the EM actuator draws the least power, the EH draws the midrange and ESH requires the most. In the elevator plot of Fig. 8, from 330 seconds onwards the EH actuator demands the most power. This is because the load force during this time is high (over 2/3 the stall force) and in this condition the ESH technology has the lowest losses.

Fig. 9 shows one power peak in detail to show how each actuator initially responds to a command; the power spike generated as the motor is started has been softened using relaxed controller gains. This is considered acceptable since the cost to manoeuvre performance is small, but the increase in simulation speed through increased solver time step size is significant.

The responses show oscillations caused by the controllers 'hunting' in the speed control loop. Efforts to alleviate this by hand tuning the controller have caused severely reduced position performance of the actuator and so have been left as shown.

| Actuator | *ode23tb* (s) |
|---|---|
| ESH | 24.8 |
| EM | 35.4 |
| EH | 22.6 |

**Tab. 4: Simulation times for each aircraft model with actuators.**

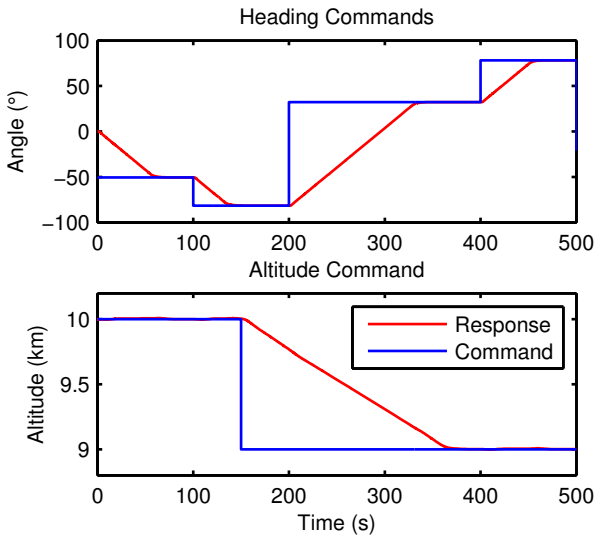


**Fig. 6. Plot of aircraft manoeuvres.**

## 7 Conclusion

'Green' operations is a topic at the forefront of commercial aviation today. Energy savings are not only to be realised through changes in aircraft design but also in operation. This research aims to cover both areas through analysis of different actuation system technologies as well as trajectory optimisation. The technologies studied range from the classical electro servohydraulic to the to the state of the art electromechanical and electro-hydrostatic actuators.

The actuation systems are modelled using the fundamental equations defining their position response and power consumption behaviour, optimised for fast execution rather than fidelity in the nonlinear region of operation. Basic nonlinearities are, however, included such as Coulomb friction, motor field saturation and pressure limitation to increase the fidelity of the models.

The actuator models are combined with a 6-DOF aircraft model with autopilot which generates control surface commands as the aircraft follows a predefined set of manoeuvres. A control surface hinge moment aerodynamic load estimator is programmed using textbook 2D methods and this is capable of producing good estimates in most of the flight conditions of a transport aircraft.

The tool is used to produce an estimate of the dynamic power consumption of each

actuator technology for a test case and achieves a speed of between 14 and 22 times faster than real time. The power consumption results mirror previous work by Di Rito et al. [3] which show the electromechanical actuator as the most efficient, the electrohydrostatic as the median and the classical electro-servohydraulic as the least efficient in most cases. Only when an actuator has to hold a high force (>2/3 stall force) at zero velocity does the classical system become more efficient than the EH actuator.

Future work proposed for the model includes:

1) Using the models described here in future Clean Sky research to provide reliable estimates of the error statistics associated with the primary flight control variables. These will then be used as an input to the trajectory optimisation process. It is envisaged that the error parameters associated with control input uncertainties in the ADM will be computed using the electrical and hydraulic actuation system models presented in his paper, towards achieving a higher level of fidelity in the aircraft trajectory estimation and optimisation process.

2) A study and optimisation of lateral manoeuvres for the minimisation of actuator energy consumption, potentially for realistic flight routes between city pairs. The drive is that although the power savings may be small, the improvements can be realised on future aircraft through minor software changes to an aircraft's flight management system.

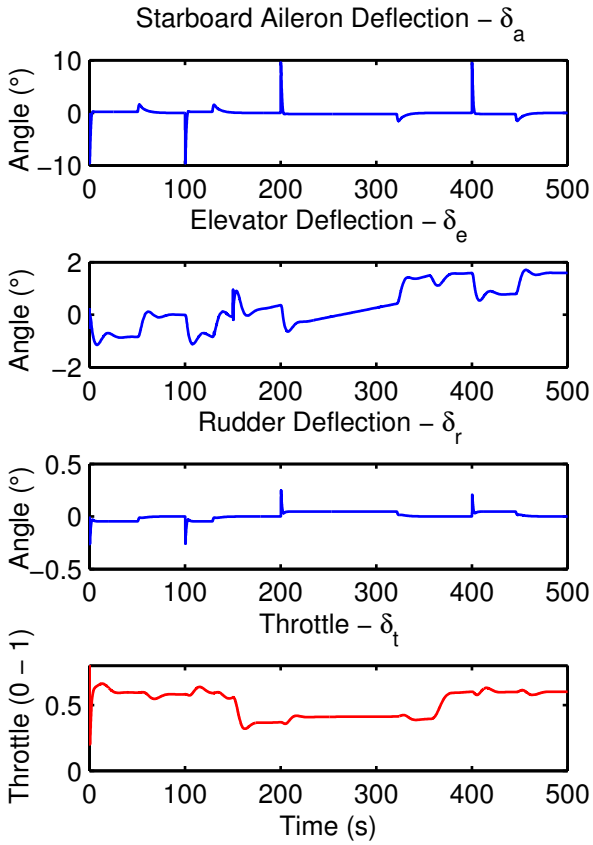


**Fig. 7. Control surface deflections during manoeuvres.**

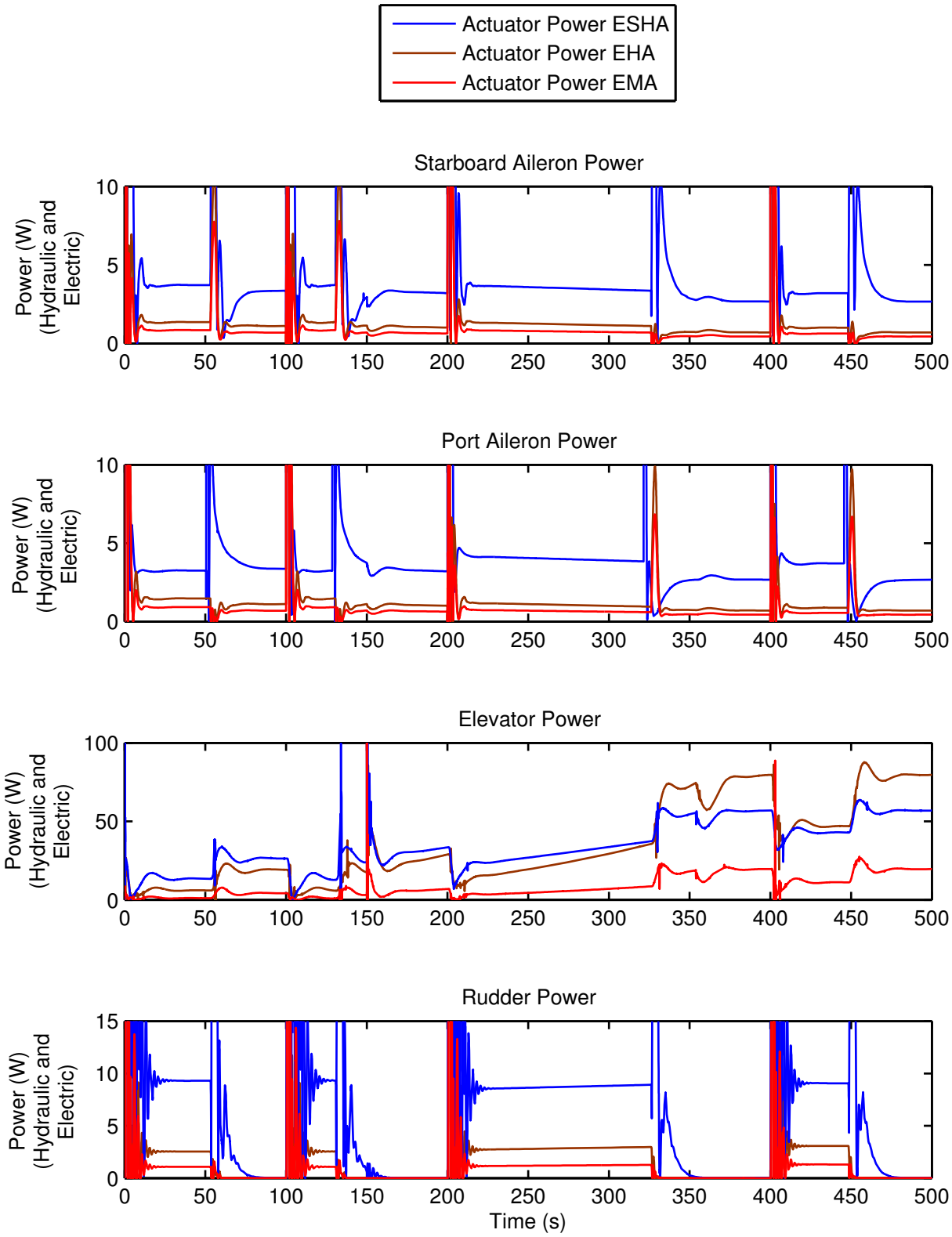


**Fig. 8. Plot of the power consumed at each actuator (hydraulic power for ESHA and electrical power for EMA and EHA).**

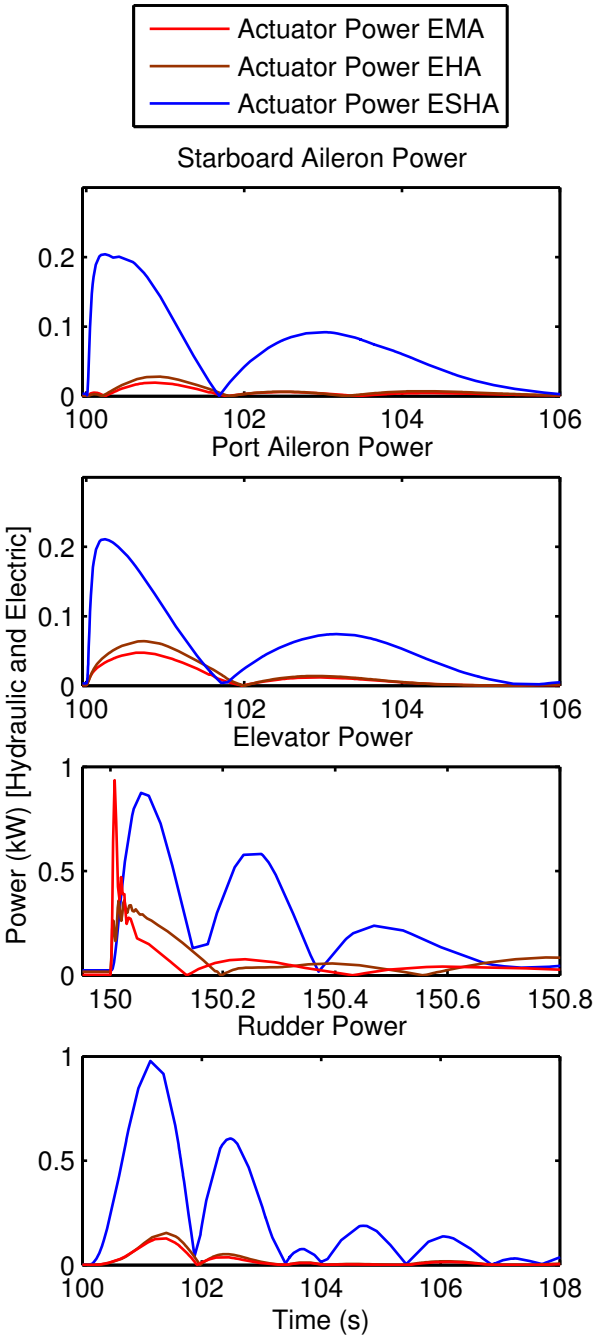


**Fig. 9. Plot showing detail of power peaks which are cropped from Fig. 8.**

## Acknowledgements

The research leading to these results received funding from the European Union's Seventh Framework Programme (FP7/2007-2013) for the Clean Sky Joint Technology Initiative under grant agreement n° CSJU-GAM-SGO-2008-001.

## References

[1] Jones R. The more electric aircraft – assessing the benefits. *Proceedings of the Institution of Mechanical Engineers, Part G: Journal of Aerospace Engineering*, Vol. 216, No. 5, pp 259-269, 2002.

[2] van den Bossche D**.** The A380 flight control electrohydrostatic actuators, achievements and lessons learnt. *Proceedings of the 25th Congress of the International Council of the Aeronautical Sciences (ICAS)*, Vol 7.4.1, Hamburg, Germany, 2006.

[3] Di Rito G, Denti E and Galatolo R. Object-oriented modelling of flight control actuation systems for power absorption assessment. *Proceedings of the 27th Congress of the International Council of the Aeronautical Sciences (ICAS)*, Vol 7.4.2, Nice, France, 2010.

[4] Dinca L, Corcau J, Lungu M and Tudosie A. Mathematical models and numerical simulations for electro-hydrostatic actuators. *International Journal of Circuits, Systems and Signal Processing*, Vol. 2, No. 4, pp 229-238, 2008.

[5] Poley R**.** *DSP Control of Electro-Hydraulic Servo Actuators*. Application Report (SPRAA76), Texas Instruments, 2005.

[6] Thayer W J**.** *Transfer functions for Moog servovalves*. Technical Note I03, Moog Inc, 1965.

[7] Du X, Dixon R, Goodall R and Zolotas A. Modelling and control of a high redundancy actuator. *Mechatronics*, Vol. 20, No. 1, pp 102-112, 2010.

[8] Roskam J**.** *Aircraft Design Vol VI*. 1st edition, Roskam Aviation & Engineering Corporation, 1987.

[9] Scholz D**.** *Equations for a preliminary actuator design*. Technical Note (TN-EV52-360/91), Deutsche Airbus, 1991.

[10] Parker Hannifin**.** *Fundamentals of Servo Motion Control*, available at: www.compumotor.com /whitepages/ServoFundamentals.pdf (accessed 1 February 2012).

[11] Moog Inc**.** *Electrohydraulic Valves... A Technical Look*, available at: www.moog.com /literature/ICD/Valves-Introduction.pdf (accessed 9 January 2012).

## Copyright Statement